THE JOURNAL OF BIOLOGICAL CHEMISTRY
Vol. 273, No. 13, Issue of March 27, pp. 7177–7180, 1998
© 1998 by The American Society for Biochemistry and Molecular Biology, Inc.
Printed in U.S.A.

Communication

Organization of HIV-1 Capsid Proteins on a Lipid Monolayer*

(Received for publication, November 25, 1997, and in revised form, January 21, 1998)

Eric Barklis‡§, Jason McDermott‡, Stephan Wilkens¶, Stephen Fuller‖, and David Thompson**

*From the ‡Vollum Institute and Department of Microbiology, Oregon Health Sciences University, Portland, Oregon 97201-3098, the ¶Institute of Molecular Biology, University of Oregon, Eugene, Oregon, 97403, the ‖Structural Biology Programme, European Molecular Biology Laboratory, D-69012 Heidelberg, Germany, and the **Department of Chemistry, Purdue University, West Lafayette, Indiana 47907*

In an *in vitro* system that mimics the assembly of immature human immunodeficiency virus (HIV) particles, ordered arrays of HIV-1 capsid (CA) proteins encoded by the viral *gag* gene have been obtained by incubation of histidine-tagged capsid proteins (His-HIVCA) beneath lipid monolayers containing the nickel-chelating lipid, 1,2-di-*O*-hexadecyl-*sn*-glycero-3-(1′-2′′-R-hydroxy-3′-*N*-(5-amino-1-carboxypentyl)iminodiacetic acid)propyl ether. The membrane-bound His-HIVCA proteins formed small crystalline arrays of primitive (p1) unit cells with dimensions of a = 74.2 Å, b = 126.2 Å, γ = 89.3°. The image-analyzed two-dimensional projection of His-HIVCA assemblies shows a cage-like lattice, consisting of hexamer and trimer units, surrounding protein-free cage holes. The hexamer-coordinated cage holes of 26.3-Å diameter are spaced at 74.2-Å intervals: these distances, and the hexamer-trimer arrangement, are consistent with previous, lower resolution studies on immature HIV-1 virus particles produced *in vivo*. Additionally, HIV-1 matrix protein trimer unit structures align to the His-HIVCA trimer units such that residues previously shown to interact with the HIV-1 gp120/gp41 envelope protein complex are oriented toward the hexamer cage holes. Our results form a bridge between results from conventional methods for the analysis of HIV particle structure.

The products of the human immunodeficiency virus (HIV-1)[1] assembly are 125-nm diameter, enveloped, immature, and mature virus particles (1). The principal internal protein component of HIV-1 virions is encoded by the viral *gag* gene. Immature HIV-1 particles are composed of unprocessed 55-kDa Gag proteins (Pr55Gag) and appear to have an electron dense layer of material juxtaposed to the inner faces of their lipid envelopes (1, 2). However, during or just after virus particle release from cells, Pr55Gag proteins are processed by the HIV-1 protease into the major mature Gag proteins matrix (MA), capsid (CA), nucleocapsid (NC), and p6. Proteolytically processed HIV-1 particles adopt a mature morphology, in which electron-dense material reorganizes into a central cone- or rod-shaped structure (1).

Complete or partial structures for the MA, NC, and CA Gag proteins have been determined in nuclear magnetic resonance spectroscopy (NMR) and x-ray crystallographic studies (3–10). The matrix protein, which interacts with the HIV-1 envelope (Env) protein complex (SU/TM or gp120/gp41) and serves a membrane binding function, forms characteristic trimers in three different crystal forms (5). The NC domain possesses two Cys-His finger motifs, which coordinate zinc ions and are important in RNA binding (10). The capsid domain, which is crucial to virus particle assembly (11), has proven more difficult. However, partial structures of HIV-1 CA have shown that it is composed primarily of α helices (6–9), an unexpected contrast with the B-barrel or jellyroll structures, which constitute the capsid proteins of a number of other animal viruses.

While NMR and x-ray structures of individual HIV-1 Gag proteins provide clues as to potential interprotein contacts within HIV-1 particles, much remains obscure. Several reports have suggested that mature and immature HIV-1 virions show icosahedral symmetry (1, 2), but high resolution support for this suggestion is needed. Analysis of mature virus cores has been hampered by difficulties in their isolation, although the recent demonstration that RNA-Gag (CA plus NC) complexes can be assembled *in vitro* (11) may lead to an accurate model for mature HIV-1 cores. However, the most developed model for the structure of HIV-1 is based on the immature virus form. In particular, examination of negatively stained membranes and immature HIV particles produced from a baculovirus vector led Nermut *et al.* (2) to propose a "fullerene-like" particle structure. By this model, Pr55Gag proteins at viral or cell membranes appear to form hexamer rings surrounding protein-free "holes." Although first order diffraction reflections at 65 $Å^{-1}$ were barely discernible, results of averaging five subimages, assuming 6-fold rotational symmetry, suggested an arrangement in which only one Pr55Gag monomer would be shared by two adjacent hexamer units (2). More recent cryo-EM analysis of disrupted HIV-1 virus-like particles also showed that Pr55Gag proteins appear to form a cage-like structure, although in this case, cage hole-to-hole distances appeared to be on the order of 48 Å (13). In our current study, we describe a method for the analysis of HIV-1 capsid proteins, assembled *in vitro* on a lipid monolayer. Our results show that membrane-bound HIV-1 CA proteins organize into a hexamer-trimer cage-like network that explains previous structural results in a consistent model.

EXPERIMENTAL PROCEDURES

Lipid Monolayer Incubations and Electron Microscopy—The His-HIVCA protein has been described previously (11) and consists of the HIV-1 coding region with an amino-terminal histidine tag and a 3.3-kDa COOH-terminal extension. The His-HIVCA protein was purified and analyzed as described previously (11, 15). For monolayer incubations, we followed our standard protocol (14) with the subphase con-

* This work was supported by American Foundation for AIDS Research and National Institutes of Health Grants 2R01 CA47088 and 5R01 GM52914 (to E. B.) and a grant from the National Science Foundation (to D. T.). The costs of publication of this article were defrayed in part by the payment of page charges. This article must therefore be hereby marked "*advertisement*" in accordance with 18 U.S.C. Section 1734 solely to indicate this fact.

§ To whom correspondence should be addressed. Tel.: 503-494-8098; Fax: 503-494-6862; E-mail: barklis@ohsu.edu.

[1] The abbreviations used are: HIV-1, human immunodeficiency virus type 1; MA, matrix; CA, capsid; NC, nucleocapsid; DHGN, 1,2-di-*O*-hexadecyl-*sn*-glycero-3-(1′-2′′-R-hydroxy-3′-*N*-(5-amino-1-carboxypentyl)iminodiacetic acid)propyl ether; FRC, Fourier ring correlation; PC, phosphatidylcholine; M-MuLV, Moloney murine leukemia virus; EM, electron microscopy.

taining 0.5–2.0 mg/ml His-HIVCA in subphase buffer at pH 7.8 or 8.3. Subphase solutions were overlayered as described (14) with 1:1 hexane: chloroform containing 200 μg/ml phosphatidylcholine (Avanti Polar Lipids) plus 50 μg/ml nickel-charged DHGN (1,2-di-*O*-hexadecyl-*sn*-glycero-3-(1′-2′′-R-hydroxy-3′-*N*-(5-amino-1-carboxypentyl)iminodiacetic acid)propyl ether). After overnight incubation at 25–30 °C, arrays were lifted onto lacey grids, washed 30 s in distilled water, and either negative-stained in 1.33% uranyl acetate or plunge-frozen in liquid ethane. Monolayer arrays were viewed and photographed at the Portland Veterans Affairs Hospital JEOL JEM12OOEX, the University of Oregon Philips CM12, or the EMBL-Heidelberg Philips CM200-FEG as described previously (14). Crystalline areas on micrographs were identified by optical diffraction, and images were scanned and digitized using either the EMBL-Heidelberg Perkin-Elmer 1010GM flat-bed scanner at 2.63 Å/pixel or an Optronics CCD mounted on a dissecting microscope at 5.25 Å/pixel. Since CM200-FEG images used in averages were taken at 900 nm defocus, corresponding to a first contrast transfer function zero of approximately 15.1 Å, contrast transfer function correction was not applied in our analyses.

Image Analysis—Image analysis steps employed both the MRC (16, 17) and SPIDER (18) image analysis packages. Initially, ordered areas, identified by optical diffraction, were scanned, converted to MRC image files, boxed using BOXMRC, Fourier-transformed, and viewed as diffraction patterns on SPECTRA (19). Diffraction patterns were indexed by hand, masked, and back-transformed to yield crude filtered images (14, 17). For more thorough analysis, SPIDER (18) real space operations were used. Twenty 168.3 Å × 168.3 Å windows, corresponding to approximately two p1 unit cells from the initial filtered images, were picked using the SPIDER operation WI from scanned negative 8347 that had been Gaussian low pass filtered to 32.9-Å resolution. The filtered windows were aligned using the AP RA and AP SA operations and averaged using the AD command. The averaged image then was used as a reference with the programs CC and PK D to pick three sets of cross-correlation peaks: 100 image windows from negative 8347; the best 280 cross-correlation peaks from five digitized negatives; and 1000 windows from the five negatives. Windows from each data set were aligned to a black and white contrast version of the averaged reference window. Aligned windows in each set were averaged using the SPIDER AD operation. For statistical analysis, data sets were halved, averaged, and compared with obtain Fourier ring correlation (FRC) indices at different rings of resolution using RF M. Image averages subsequently were filtered using FQ to 24.0 Å resolution in accordance with FRC results.

For rotational averaging, a rotational series of the averaged, negative 8347 data set was generated using RT, and rotated images were compared with the unrotated original using RF M, identifying rotational correlation peaks. The original plus its 60, 120, 180, 240, and 300° rotations were averaged to give a rotationally averaged image: the FRC of the 0, 120, and 240° average *versus* the 60, 180, and 300° average was 0.90 at 36.0 Å resolution and 0.62 at 22.4 Å resolution. To simulate the lower resolution obtained in previous studies, the 6-fold rotationally averaged image was Gaussian low pass filtered to 52.6 Å resolution using the FQ operation. For alignment of HIV-1 matrix protein trimers onto His-HIVCA arrays, the MA trimer unit from the Brookhaven Protein Data Bank (accession number 1H1W) was imaged on MIDAS, rotated so that the 3-fold axis was normal to the projection and the predicted internal face of the virus (4, 5), and scaled. The scaled MA trimer image was converted to SPIDER image format, used to generate a 120° rotational series of windows at 1° intervals, and each rotated trimer was cross-correlated to the six-fold rotationally averaged His-HIVCA image. The best alignment had the highest value cross-correlation peak. For display purposes, all images were converted from either MRC or SPIDER image formats to TIFF files and displayed using Adobe Photoshop software.

RESULTS AND DISCUSSION

To circumvent difficulties that have limited the structural analysis of HIV-1 particles, we have adapted the lipid monolayer method of two-dimensional protein crystallization (22) for analysis of HIV-1 Gag protein interactions. To do so, lipid monolayers were made from phosphatidylcholine (PC) plus a dialkylglycerol derivative, DHGN, which carries a nickel-chelating head group that binds histidine-tagged (His-tagged) proteins (14). The HIV-1 Gag protein chosen for analysis, His-HIVCA, was an HIV-1 (HXB2) capsid protein derivative with an amino-terminal His tag (11). Our rationale for using the matrix-deleted His-HIVCA protein was that the His tag-DHGN interaction should substitute for the membrane binding function of MA. Furthermore, studies have shown that large HIV-1 *matrix* deletions are compatible with virus particle assembly (19, 20). Although His-HIVCA also lacks the NC and p6 COOH-terminal domains of Pr55Gag, this did not prevent his-HIVCA from mimicking interactions observed for the full-length protein (see below).

The recombinant His-HIVCA protein was produced in *Escherichia coli* and purified to greater than 95% homogeneity by two rounds of nondenaturing nickel-chelate chromatography (15). As a conformation check, His-HIVCA and HIV-1 CA isolated from virus particles were subjected in parallel to a partial proteolytic treatments, and each protein yielded a characteristic COOH-terminal 14-kDa partial trypsin fragment. When His-HIVCA proteins were used in monolayer incubations with PC plus DHGN, protein arrays with small patches of crystallinity were observed with either stained samples (Fig. 1*A*) or samples frozen in vitreous water. While such regions could be difficult to detect in cryo-EM micrographs (see Fig. 1*B*), they were evident in low pass filtered cryo-EM images (Fig. 1*C*). In small regions, His-HIVCA proteins were ordered well enough to obtain distinct diffraction patterns, as shown in Fig. 1*D*. Despite sample drift for this negative, the reflections at 26.1 $Å^{-1}$ are clearly evident, and the primitive (p1) unit cell of a = 74.8 Å, b = 126.2 Å, γ = 89.3° is reminiscent of the a = 79.2 Å, b = 137.5 Å, γ = 89.7° unit cell observed for capsid proteins of another retrovirus, the Moloney murine leukemia virus (M-MuLV) (1, 14). Interestingly, back-transformation of masked diffraction patterns from small ordered regions yielded images (Fig. 1*E*) showing a cage-like structure of proteins (light) surrounding protein-free cage holes (dark), similar to those seen for M-MuLV CA (14) and HIV-1 Pr55Gag (2).

Because the sizes of ordered His-HIVCA patches were not large enough to permit a thorough analysis by standard diffraction analysis methods (16, 17), we opted to analyze His-HIVCA monolayer structures by a modification of single particle analysis methods (18). To do so, an image-averaged reference corresponding to approximately two p1 unit cells (168.3 Å × 168.3 Å) was used to locate cross-correlation peaks from five separate digitized micrographs. As expected from the low pass filtered image (Fig. 1*C*), peaks tended to be located in small ordered patches throughout the micrographs (Fig. 1*F*). From cross-correlation maps, three data sets were derived. These consisted of 100 image windows from our highest quality micrograph, 280 windows corresponding to the best cross-correlation peaks, and 1000 windows (total) from the five micrographs. All windows were aligned to a black and white averaged reference window, after which data sets were merged to obtain 100-image, 280-image, and 1000-image averages (Fig. 2, *A–C*). To evaluate results, each data set was halved, and averages from each half set were compared with their counterparts at different rings of resolution. As shown in Table I, for each data set, Fourier ring correlation values fall off at resolutions better than 24.0 Å. These results are consistent with the observation of reflections at 26.1 $Å^{-1}$ (Fig. 1*D*), and Figs. 2, *D–F*, have been filtered to this resolution limit.

The most obvious features of the His-HIVCA structures shown in Fig. 2 are the large circular holes of 26.3 Å in the protein cage, which are bordered by six rectangularly shaped protein units. However, each circular hole also is surrounded by six smaller protein-free zones, which in turn are bordered by three rectangular units. Thus, membrane-bound HIV-1 capsid appears to form a cage consisting of hexamer and trimer units. Since previous lower resolution studies on *in vivo* derived immature HIV-1 particles employed a 6-fold rotational averaging

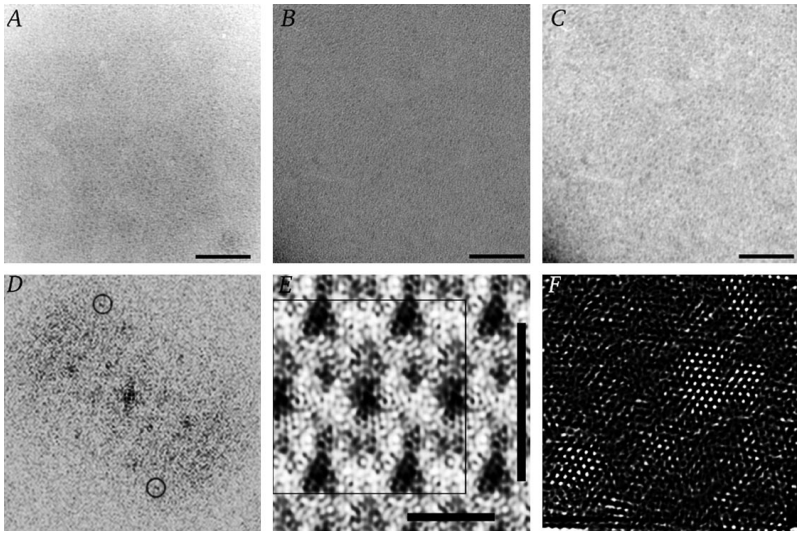

FIG. 1. **Two-dimensional arrays of His-HIVCA on lipid monolayers.** *A*, negatively stained His-HIVCA array formed on PC plus DHGN. The contrast on the scanned EM negative was inverted so that protein-free regions are *dark*. The *scale bar* is 53.6 nm. *B*, unfiltered cryo-EM image of His-HIVCA arrays. Protein-free regions appear *dark*, and the *size bar* indicates 50 nm. *C*, the image from *B* was Gaussian low pass filtered to 32.9 Å resolution using the SPIDER operation FQ. The *size bar* indicates 50 nm. *D*, the power spectrum from a 135 × 135-nm His-HIVCA array in vitreous ice was calculated from the scanned image and can be indexed as a primitive (p1) unit cell with a = 74.8 Å, b = 126.2 Å, γ = 89.2°. The *circled* 2,−4 and 2,4 reflections are at 26.1 $Å^{-1}$. *E*, the calculated diffraction pattern from an ordered section of negative 8347 was displayed, indexed, and masked using SPECTRA (18) and back-transformed to yield the filtered image, in which protein-free areas appear *dark*, while electron-dense areas are *bright*. The *thick black lines* indicate p1 unit cell dimensions of 74.8 and 126.2 Å, while the *thin black line* shows the box format used to pick windows to average for the cross-correlation reference in *F*. *F*, *white spots* indicate cross-correlation peaks from *B*, using a reference averaged from 20 168.3 × 168.3-Å negative 8347 windows that were *boxed* using the two-unit cell box from *E* as a guide.

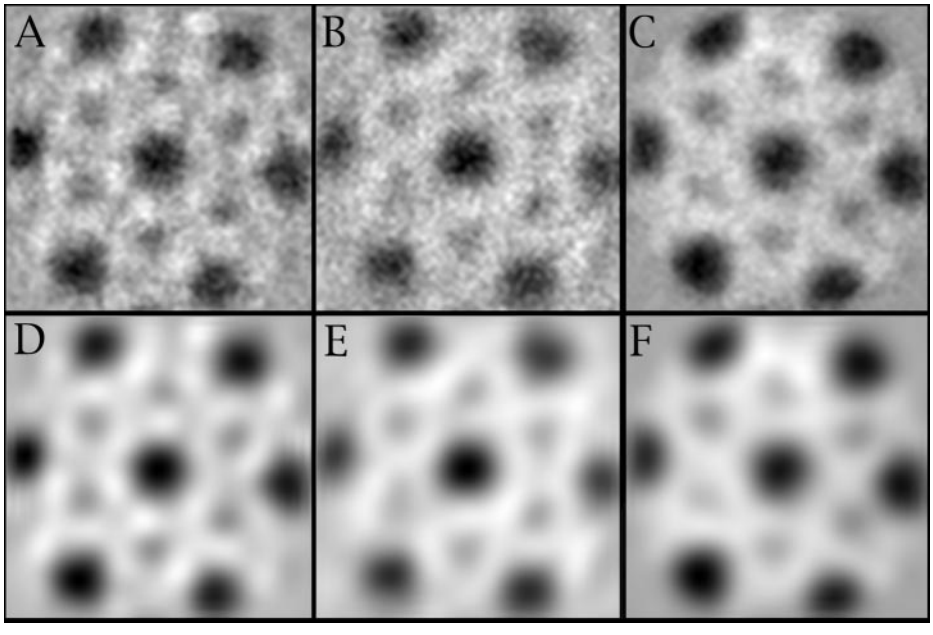

FIG. 2. **Arrangement of HIV-1 capsid proteins bound to a lipid monolayer.** Image windows from cryo-EM micrographs of two-dimensional His-HIVCA arrays were aligned and averaged as described under "Materials and Methods." Averages are displayed as 168.3 × 168.3-Å areas with protein-free zones *dark* and electron-dense areas *light*. Averages were either unfiltered, or Gaussian low pass filtered to 24.0-Å resolution, in accordance with results from Table I. *A*, 100-window average, unfiltered; *B*, 280-window average, unfiltered; *C*, 1000-window average, unfiltered; *D*, 100-window average, filtered; *E*, 280-window average, filtered; *F*, 1000-window average, filtered.

TABLE I
Phase residual and Fourier ring correlation (FRC) values of averaged data sets at different resolution ranges

Resolution range	FRC		
	100-Image	280-Image	1000-Image
Å			
≥168.3	0.88	0.95	0.99
168.3–56.1	0.95	0.99	0.99
56.1–33.7	0.92	0.96	0.97
33.7–24.0	0.61	0.69	0.73
24.0–18.7	0.16	0.06	0.29

scheme in image reconstructions (2), we wished to assess the results of rotational averaging for comparative purposes. As shown in Fig. 3*A* (*top panel*), the large cage holes in the HIV-1 capsid arrays appeared as 6-fold rotational axes, and the averaged image correlated with its 60° rotation to about 21.3 Å (Fig. 3*A, bottom panel*). Six-fold averaging increased the distinction of putative monomer units (Fig. 3*B*), and when this image was filtered to 52.6 Å resolution, the four rectangular units separating each trimer hole appeared as single electron-dense units (Fig. 3*C*). The resultant image compares well with HIV-1 Pr55Gag arrays at membranes and in disrupted immature virus particles (2, 13). In particular, the 74.2-Å hexamer to hexamer cage hole spacing that we observe (Figs. 2 and 3) is consistent with the spacing observed for Pr55Gag proteins arranged on the plasma membranes of baculovirus vector-infected cells (2). Since that study used negatively stained samples and was at low resolution, we believe that trimer cage holes were not resolved, much as they are not resolved in our

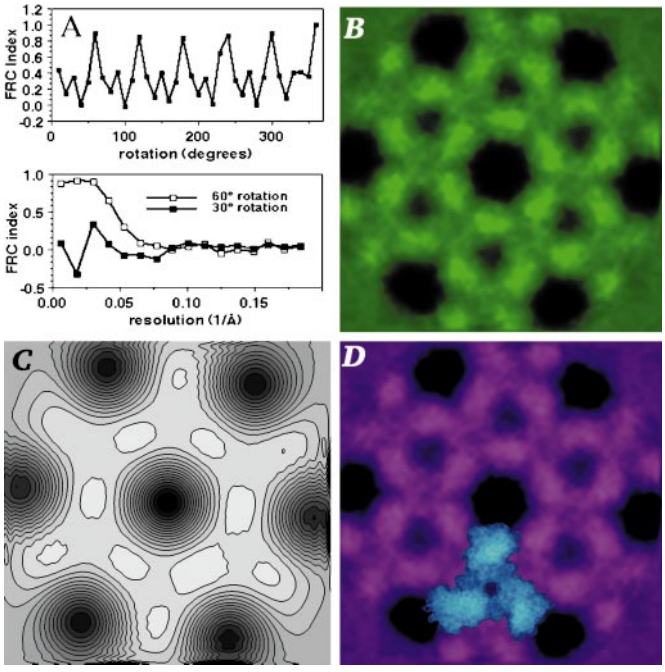

FIG. 3. **Rotational averaging and comparison with virus particle and atomic structures.** *A, top panel*, the unfiltered average from Fig. 2*A* was used to generate a 360° rotational series of images, which were compared with the original, unrotated average. Fourier ring correlation (FRC) values at 33.7-Å resolution were plotted *versus* rotation angles and show six peaks. *Bottom panel,* the averaged image from Fig. 2*A* was compared with 30° (*filled squares*) or 60° (*open squares*) rotated versions of itself, and results of the comparisons were plotted as FRC indices *versus* resolution in reciprocal space. For the 60° comparison, the FRC was 0.5 at 21.3 Å. *B*, the 6-fold rotationally averaged image from the 100-window data set is shown with *dark* protein-free zones and electron-dense areas in *green*. The image size is 168.3 × 168.3 Å. *C*, to simulate lower resolution results obtained with immature HIV-1 virus-like particles produced *in vivo* (2), the rotationally averaged image from *B* was filtered to 52.6-Å resolution. *D*, the HIV-1 matrix protein trimer structure (5) (Brookhaven Protein Data Bank accession number 1H1W) in *blue* was scaled and fitted with the His-HIVCA image (*purple*) to maximize projection overlap as described under "Materials and Methods." After identification of the best-fit cross-correlation peak, the scaled matrix trimer, depicted as a space-filling model, was oriented so that its predicted membrane-binding face (4, 5) is away from the reader. In this representation, matrix residues 11–32 and 87–100 are oriented toward hexamer holes, where HIV-1 gp120/gp41 envelope protein complex cytoplasmic tails have been postulated to reside (2).

low pass filtered image (Fig. 3*C*). In contrast, cryo-EM analysis of disrupted immature HIV-1 particles has shown a cage hole center-to-center spacing of approximately 48 Å (13), which is in good agreement with our observation of trimer to hexamer cage hole spacing of 44.9 Å. Given the above observations, it appears that membrane-bound HIV-1 CA proteins assemble in a fashion similar to the full-length Pr55Gag proteins. This may seem surprising, since Gag protein nucleocapsid (NC) domains, possibly through associations with RNA, exert a strong influence on retrovirus particle assembly (12, 14). However, the similarity of our HIV-1 CA projection structure (Figs. 2 and 3), and that of Pr55Gag proteins in virus-like particles (2), is consistent with indications that MA, CA, and NC domains in Pr55Gag molecules stack roughly as long rods (13). We thus hypothesize that NC and RNA interactions do not alter the basic arrangements of membrane-tethered capsid proteins, at least at our level of detection.

Although the HIV-1 CA hexamer-trimer arrangement agrees with available data on immature HIV-1 patches, it differs slightly from the hexamer-hexamer arrangement, which M-MuLV capsid proteins form on membrane monolayers (14). In particular, M-MuLV capsid proteins form arrays in which roughly symmetrical hexamer cage holes are surrounded by six skewed hexamer cage holes. Also, in contrast with HIV-1 CA arrays, in which each monomer unit contributes to one hexamer and one trimer, M-MuLV monomer units each contribute to one symmetrical and two skewed cage holes (14). Furthermore, at hexamer vertices, it appears that putative HIV-1 CA monomers coordinate with three other monomer units, while M-MuLV monomers coordinate only with two additional monomers. However, both M-MuLV and HIV-1 arrangements suggest that cytoplasmic portions of the retroviral Env proteins may be accommodated in the hexamer cage hole regions. For HIV, if this is the case, then one might expect that the Pr55Gag matrix domains ordinarily should be positioned between the viral membranes and the CA domains. In keeping with this hypothesis, when HIV-1 matrix trimers as observed in three-dimensional crystals were oriented toward viral membranes as predicted previously (3–5) and scaled to our projection structure, they overlaid neatly onto the capsid trimer units (Fig. 3*D*). In this structure, matrix residues 11–32 and 87–100 are oriented toward hexamer holes and could interact with the cytoplasmic tails of HIV-1 gp120/gp41 Env protein trimers (21), which have been postulated to localize to cage holes (2). While the extent to which our system mimics authentic HIV assembly is unclear, we believe that our results, will help identify protein-protein interactions in HIV virions that can be targeted for antiviral therapies.

Acknowledgments—We are grateful for the help we have received from Lori Farrell, Sonya Karanjia, Jenny Stegeman-Olsen, Mike Yamauchi, Yuanjui Rui, Xiumin Zhao, Brent Gowen, Russell Jones, Charles Meshul, Eric Schabtach, Dick Brennan, Darrick Carter, Mike Schmid, and Jackson Shea.

REFERENCES

1. Gelderblom, H. R. (1991) *AIDS* **5,** 617–638
2. Nermut, M., Hockley, D., Jowett, J., Jones, I., Garreau, M., and Thomas, D. (1994) *Virology* **198,** 288–296
3. Matthews, S., Barlow, P., Boyd, J., Barton, G., Russell, R., Mills, H., Cunningham, M., Meyers, N., Burns, N., Clark, N., Kingsman, S., Kingsman, A., and Campbell, I. (1994) *Nature* **370,** 666–668
4. Rao, Z., Belyaev, A., Fry, E., Roy, P., Jones, I., and Stuart, D. (1995) *Nature* **378,** 743–747
5. Hill, C., Worthylake, D., Bancroft, D., Christensen, A., and Sundquist, W. (1996) *Proc. Natl. Acad. Sci. U. S. A.* **93,** 3099–3104
6. Gitti, R., Lee, B., Walker, J., Summers, M., Yoo, S., and Sundquist, W. (1996) *Science* **273,** 231–235
7. Momany, C., Kovari, L., Prongay, A., Keller, W., Gitti, R., Lee, B., Gorbalenya, A., Tong, L., McClure, J., Ehrlich, L., Summers, M., Carter, C., and Rossmann, M. (1996) *Nat. Struct. Biol.* **3,** 763–770
8. Gamble, T., Vajados, Yoo, S., Worthylake, D., Houseweart, M., Sundquist, W., and Hill, C. (1996) *Cell* **87,** 1285–1294
9. Gamble, T., Yoo, S., Vajdos, F., von Schwedler, U., Worthylake, D., Wang, H., McCutcheon, J., Sundquist, W., and Hill, C. (1997) *Science* **278,** 849–853
10. Morrelet, N., Jullian, N., De Rocquigny, H., Maigret, B., Darlix, J.-L., and Roques, B. (1992) *EMBO J.* **11,** 3059–3065
11. McDermott, J., Farrell, L., Ross, R., and Barklis, E. (1996) *J. Virol.* **70,** 5106–5114
12. Campbell, S., and Vogt, V. (1995) *J. Virol.* **69,** 6487–6497
13. Fuller, S., Wilk, T., Gowen, B., Krausslich, H.-G., and Vogt, V. (1997) *Curr. Biol.* **7,** 729–738
14. Barklis, E., McDermott, J., Wilkens, S., Schabtach, E., Schmid, M., Fuller, S., Karanjia, S., Love, Z., Jones, R., Rui, Y., Zhao, X., and Thompson, D. (1997) *EMBO J.* **16,** 1199–1213
15. Hochuli, E., Dobeli, H., and Schacher, A. (1987) *J. Chromatogr.* **411,** 177–184
16. Crowther, R., Henderson, R., and Smith, J. (1996) *J. Struct. Biol.* **116,** 9–16
17. Hardt, S., Wang, B., and Schmid, M. F. (1996) *J. Struct. Biol.* **116,** 68–70
18. Frank, J., Radermacher, M., Penczek, P., Zhu, J., Li, Y., Ladjadj, M., and Leith, A. (1996) *J. Struct. Biol.* **116,** 190–199
19. Faecke, M., Janetzko, A., Shoeman, R., and Krausslich, H.-G. (1993) *J. Virol.* **67,** 4972–4980
20. Wang, C., Zhang, Y., McDermott, J., and Barklis, E. (1993) *J. Virol.* **67,** 5550–5561
21. Chan, D., Fass, D., Berger, J., and Kim, P. (1997) *Cell* **89,** 263–273
22. Uzgiris, E., and Kornberg, R. (1983) *Nature* **301,** 125–129